X-ray diffraction from a coherently illuminated Si(001) grating surface

Qun Shen
Cornell High Energy Synchrotron Source and School of Applied and Engineering Physics, Cornell University, Ithaca, New York 14853

C. C. Umbach, B. Weselak, and J. M. Blakely
Department of Materials Science and Engineering, Cornell University, Ithaca, New York 14853
(Received 21 May 1993; revised manuscript received 5 August 1993)

High-resolution synchrotron x-ray diffraction from a Si(001) grating surface reveals resolution-limited grating interference peaks around each Bragg reflection. The peaks can be explained by kinematic scattering theory using the concept of a grating form factor. The positions and the intensities of the satellite peaks yield structural information such as the period, the width, and the height of the gratings, as well as its shape and its orientation and registry with respect to substrate lattice, and possible crystal strains.

In recent years x-ray diffraction has emerged as a useful tool for studying crystal surface and interface structures with microscopic, atomic scale sensitivity.[1] Special properties of the x-ray technique, such as its kinematic scattering and nondestructive nature, and the high resolution and high intensity available nowadays with synchrotron radiation, have all been beneficial to various applications in surface structural analysis. In this paper, we demonstrate another important aspect of x-ray scattering from crystal surfaces. We show that with a good transverse coherence length, x-ray scattering not only is sensitive to *microscopic* crystal structures but also allows one to study the *mesoscopic* features of surface grating or other charge-density modulations that have periodicities on the order of $\leq 1\ \mu$m.

Submicrometer- or nanometer-sized structures on semiconductor surfaces have attracted great interest recently because of their potential applications in electronic and optoelectronic devices.[2] The band structure of a semiconductor crystal may be affected significantly by quantum confinement, raising the possibilities that unusual and ultrasmall optoelectronic devices may find a place in semiconductor technology. Another area that uses submicron grating structures is in the study of atomic kinetics involving surface diffusion and step arrangements.[3,4] This kind of study is related to epitaxial or heteroepitaxial growth on stepped and terraced semiconductor surfaces.[5] In all these areas, structural information on the gratings is crucial for understanding the physics of the quantum and surface effects.

To date, optical diffraction using lasers and scanning electron microscopy have been the primary methods of characterizing surface grating structures. On an atomic scale the scanning tunneling microscope can reveal detailed step and terrace structures on a grating surface.[4] Compared to all these methods, x-ray scattering is a natural extention of optical diffraction for characterizing shorter-wavelength gratings with higher spatial resolution. It has the unique ability to distinguish the underlying crystal structures from surface amorphous layers and allows one to study buried interface structures. As we will demonstrate, the x-ray scattering technique can also provide atomic registry information such as the orientation of the grating lines with respect to the crystal lattice of the grating material.

The kinematic theory of x-ray scattering from a mesoscopic grating array on a single-crystal surface can be derived in a straightforward way, entirely analogous to Bragg diffraction from an atomic lattice in a crystal.[6] Let us consider a two-dimensional (2D) grating surface in the (x,y) plane with periods (L_x, L_y), as illustrated in Fig. 1(a). In place of the atomic scattering form factor, we define a *pillar scattering form factor* as a function of $\mathbf{Q}$, the momentum transfer:

$$f_p(\mathbf{Q})=\int \rho_p(\mathbf{r})e^{i\mathbf{Q}\cdot\mathbf{r}}d\mathbf{r}\ , \qquad (1)$$

where $\rho_p(\mathbf{r})$ is the charge density of a single grating pillar. The structure factor of this pillared surface is thus

$$F(\mathbf{Q})=\Sigma_j f_p(\mathbf{Q})e^{i\mathbf{Q}\cdot\mathbf{r}_j}=f_p(\mathbf{Q})\Sigma_j e^{i\mathbf{Q}\cdot\mathbf{r}_j}\ , \qquad (2)$$

where the summation index j refers to the jth pillar and runs through the coherent crystal domain. In Eq. (2) we have omitted the scattering from the substrate, since we are mainly interested in the superlattice reflections. Assuming that $N\times N$ grating periods are illuminated coherently by the x rays, we obtain that the diffracted intensity is proportional to

$$|F(\mathbf{Q})|^2=|f_p(\mathbf{Q})|^2\left[\frac{\sin(NQ_xL_x/2)}{\sin(Q_xL_x/2)}\right]^2 \times\left[\frac{\sin(NQ_yL_y/2)}{\sin(Q_yL_y/2)}\right]^2 . \qquad (3)$$

Equation (3) describes the same diffraction pattern as in the case of Fraunhofer multiple slits diffraction in optics.[7] The standard interference function gives rise to sharp grating peaks separated by $2\pi/L_x$ and $2\pi/L_y$, with their intensities modulated by the scattering form factor $f_p(\mathbf{Q})$ from a single pillar of charge density $\rho_p(\mathbf{r})$. The form factor $f_p(\mathbf{Q})$ is peaked at each Bragg point in re-

0163-1829/93/48(24)/17967(5)/$06.00 ©1993 The American Physical Society

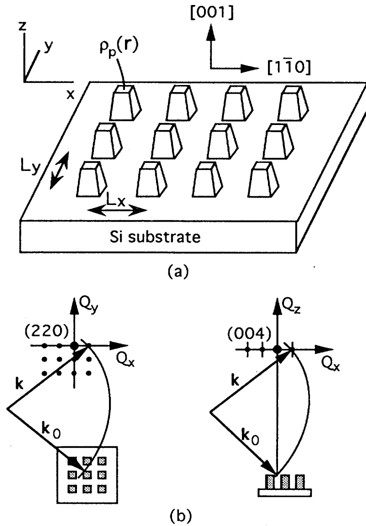

FIG. 1. (a) Schematic of a silicon (001) 2D-grating surface. (b) Two configurations of x-ray diffraction used in the experiment: the symmetric reflection geometry (right) and the glancing-angle geometry (left). The incident and the diffracted wave vectors are represented by $\mathbf{k}_0$ and $\mathbf{k}$, respectively.

ciprocal space, and is broadened by the well-known crystal size effect or crystal truncation rods,[8–10] according to the shape and the size of each pillar. Its broadness in the Q_x and Q_y directions is determined by the pillar widths, whereas its dimension in Q_z is directly related to the height of each pillar.

X-ray-diffraction studies of surface gratings have been reported in the literature using conventional laboratory x-ray sources.[11,12] Compared to a conventional source, naturally collimated and intense synchrotron radiation can provide an increase in transverse coherence length, and enhancement in brightness. This increase in coherent length has, for example, enabled the observation of "speckle" diffraction pattern arising from the interference among mosaic crystal domains.[13] For a periodic structure the interference peaks should be more easily visible. We have therefore conducted a high-resolution diffraction experiment on a 2D Si(001) surface grating sample with a nominal period of 0.3 μm, using 10-keV bending magnet radiation at the F-3 station of the Cornell High Energy Synchrotron Source (CHESS). With a vertical source size of ~ 1 mm, and a source-to-sample distance of ~ 22 m, we calculated a transverse coherence length[7,13] $L_{\mathrm{coh}} \sim 3\ \mu$m.

The grating sample was fabricated by electron-beam lithography on a Si(001) wafer at the National Nanofabrication Facility. A scanning electron micrograph (SEM) on a similarly made, cleaved grating surface is shown in Fig. 2. The 2D-grating lines are nominally parallel to the [110] and the [1$\bar{1}$0] directions and cover a 3×3 mm^2 surface area. During the x-ray experiment, which was done in air, the sample was mounted at the center of a standard four-circle diffractometer. The incident x-ray beam was monochromated by a pair of Si(111) single crystals with a sagittally focused second crystal. An x-ray flux of 10^{11} photons/sec in a 2×1 mm^2 beam size was typical

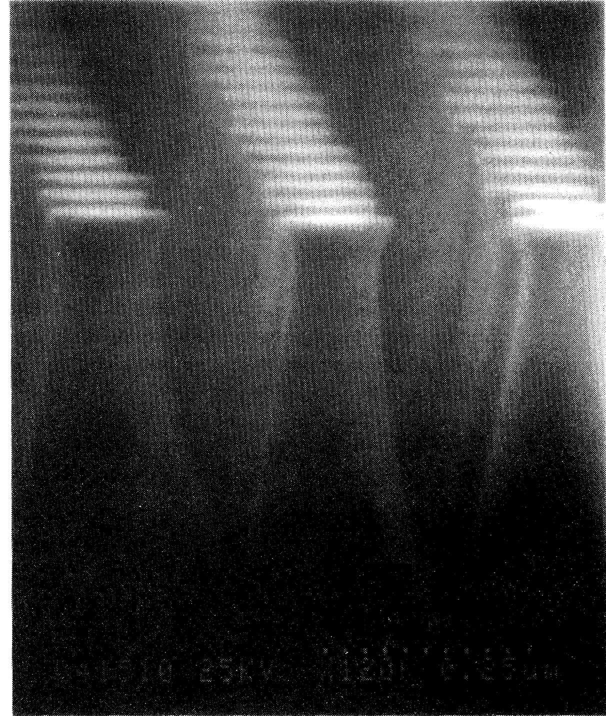

FIG. 2. A scanning electron micrograph (SEM) of a typical Si(001) grating surface studied in our x-ray-diffraction experiment. The nominal period of the grating is 0.3 μm.

during our experiment. A silicon (111) perfect crystal analyzer was used on the 2θ arm, before a NaI detector, in a nondispersive $(+,-,+)$ arrangement with the monochromator and the sample. Around the Si(220) Bragg reflection, the resolution function was determined to be $\Delta Q_\theta \le 1.2\times 10^{-4}$ Å^{-1} in the transverse, $\Delta Q_{\theta-2\theta} = 6\times 10^{-4}$ Å^{-1} in the longitudinal, and $\Delta Q_\chi \approx 2\times 10^{-2}$ Å^{-1} in the out-of-plane directions.

Two types of diffraction data were collected [Fig. 1(b)]. For lateral structural information, scans parallel to the surface were obtained near the (220) Bragg peak in the glancing-angle geometry. For height and shape information on the gratings, we did scans along the rods perpendicular to the sample surface. This was done around the (004) peak in order to take advantage of the better inplane resolution.

In Fig. 3 we show the experimental data near the (220) reflection in both the $\hat{\mathbf{x}}=[1\bar{1}0]$ and the $\hat{\mathbf{y}}=[110]$ directions. The extremely sharp and strong satellite peaks surrounding the (220) result from interference of scattered radiation from grating periods coherently illuminated by the incident beam. The satellite peaks are separated by a reciprocal period, τ, equal to $2\pi/L$. Using Eq. (3) plus a Lorentzian background due mainly to thermal diffuse scattering, we found that a coherent length of $N=20$ and a Lorentzian pillar form function $f_p(\mathbf{Q})$ can fit the data very well, as shown by the solid curves in Fig. 3. The peak positions yielded a grating period, $L = 2990\pm 10$ Å in both the $\hat{\mathbf{x}}$ and the $\hat{\mathbf{y}}$ directions. From the width of the Lorentzian envelope we obtained a full width at half maximum (FWHM) of the grating pillars, $W = 1450\pm 100$ Å.

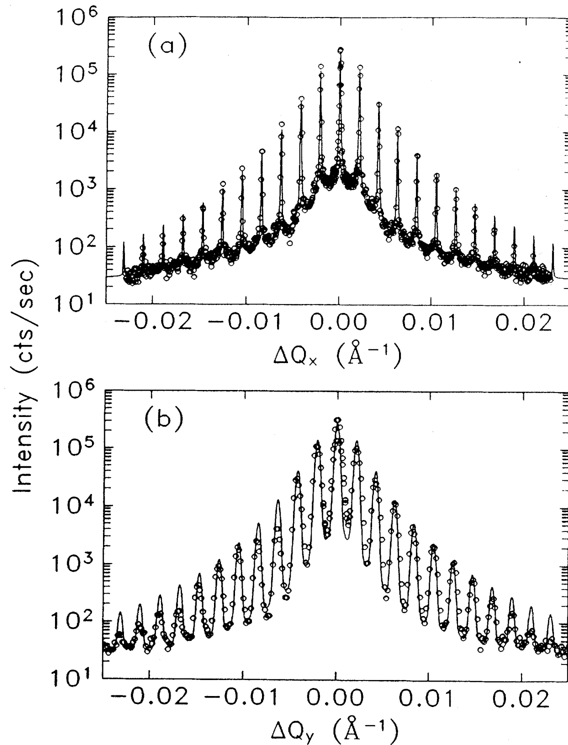

FIG. 3. High-resolution x-ray-diffraction pattern from a silicon (001) 2D-grating surface. The data (open circles) were collected around the reciprocal lattice position (2, 2, 0.04) in the grazing-angle geometry, scanning along [1$\bar{1}$0] in (a) and along [110] in (b). The solid curves are the calculations using Eq. (3), with the one in (b) being convoluted with an instrumental resolution function. The envelope profile of the grating peak intensities is determined by the width of each pillar.

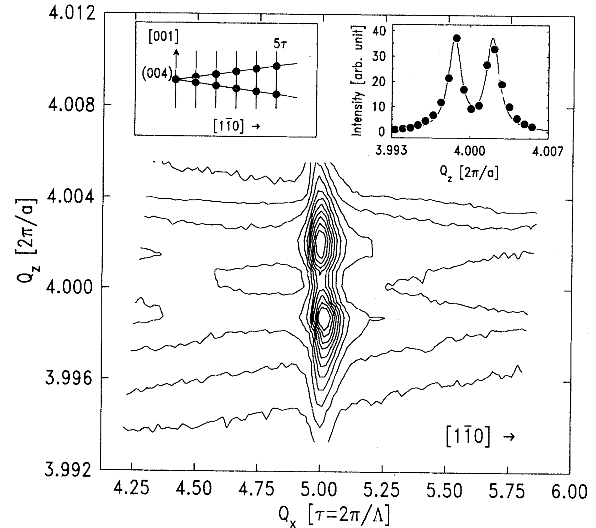

FIG. 4. Intensity contour plot around the $(5\tau/\sqrt{2}, -5\tau/\sqrt{2}, 4)$ grating peak, showing the double-peak structure due to the crystal truncation rods arising from the side walls of the grating pillars. The lattice constant $a = 5.4307$ Å, and the grating wavelength $L = 2990$ Å. There are 11 contours between intensity levels of 5000 and 40 000 with a logarithmic increment. The left inset illustrates that the diffraction peaks occur at intersections of grating interference rods and crystal truncation rods. The right inset shows the intensities integrated over Q_x, with background subtracted. The solid curve is a double-Lorentzian fit to the data. The peak width is related to the height of the pillars.

In principle, a perfect square-wave grating structure would give rise to strong modulations or missing orders in its diffraction pattern.[7] The fact that we have observed no strong modulations through the tenth-order satellite peak indicates a rounded pillar shape with sloped side walls, which agrees with the image in Fig. 2.

The rod scans along the surface normal direction (Q_z) were collected around the $(5\tau/\sqrt{2}, -5\tau/\sqrt{2}, 4)$ grating reflection, and the results are shown in Fig. 4 in the form of an intensity contour plot. We can clearly observe a double-peak pattern with almost equal intensity in the Q_z direction. The measurements at the (004) and at other grating peaks indicate that the peak splittings seem to decrease at lower-order grating peaks and approach zero at the (004) Bragg spot [see Fig. 5(a)]. Furthermore, a Q_z scan at $(4.5\tau/\sqrt{2}, -4.5\tau/\sqrt{2}, 4)$ between the fourth and fifth grating peaks also exhibits a double-peak structure, with less intensity. From these measurements we conclude that the double-peak diffraction pattern is due to the crystal truncation rods arising from the side walls of the grating pillars. According to Eq. (3), the diffracted intensity is determined by the product of a grating interference function and a form factor, $f_p(\mathbf{Q})$, from a single pillar. We therefore expect to see (left inset in Fig. 4) diffraction peaks at the intersections of the surface grating interference rods, which are along Q_z, and the crystal truncation rods in $f_p(\mathbf{Q})$, which are along the directions normal to the sidewall surface depending on the shape of the pillars. For rounded sidewalls the peak location across the truncation rod indicates the predominant slope of the sidewall surface. From the separation between the two peaks in Fig. 4 we obtained a predominant surface slope angle $\alpha = 10.4°$ with respect to the [001] surface normal for our sample. There is some indication that the side wall slopes may not be symmetric with respect to the [110] axis; we believe this is due to a slight miscut of the substrate surface. The roughness on the grating side walls may affect its truncation-rod intensity, especially at large momentum transfers away from the Bragg peaks. If it is uncorrelated from one grating period to another, the roughness would cause a decrease in the diffracted intensity at large values of ΔQ_x or ΔQ_y. This factor may be partly responsible for the discrepancy between the theoretical calculations and the experimental data at higher-order grating reflections in Fig. 3.

The diffracted intensities that are purely due to the grating interference can be obtained by taking the integrated intensities in the Q_x direction and subtracting a sloped truncation-rod background at each Q_z position in Fig. 4. Such intensities are shown in the right inset in Fig. 4. From the widths of the peaks we obtain a first-order estimate of 4900 Å for the height of the grating pillars. [The separation of the peaks cannot be explained in terms of interference between the tops and bottoms of the

grating structure; such an explanation would lead to a pillar height of ~2000 Å, which is less than the value from the SEM study (Fig. 2) by more than a factor of 2.] Taking the height as 4900 Å, along with the slope angle of 10.4° on the side walls, we reconstructed the grating pillar shape with a trapezoid approximation [Fig. 5(b)] and calculated the grating form factor $f_p(\mathbf{Q})$ for the trapezoid shape using Eq. (1), and then the diffracted intensity using Eq. (3). The results are shown as solid curves in Fig. 5(a), for the fourth-, fifth-, and sixth-order grating peaks around the (004). A Lorentzian term is added to each curve to account for the thermal diffuse scattering background. A single factor is used in the vertical axis for all three peaks so that the relative intensities among them are faithfully maintained. From Fig. 5 one can observe clearly the effect of the crystal truncation rod from the slope side walls, which causes the peak splitting to increase with the grating order. This increase also cannot be explained in terms of interference between the top and the bottom interfaces of the grating layer. The good agreement between our theory and the experiment and that between the reconstructed shape and the SEM image confirm our crystal truncation-rod theory and illustrate that detailed structural analyses of the grating forms are indeed possible using the technique of high-resolution x-ray diffraction.

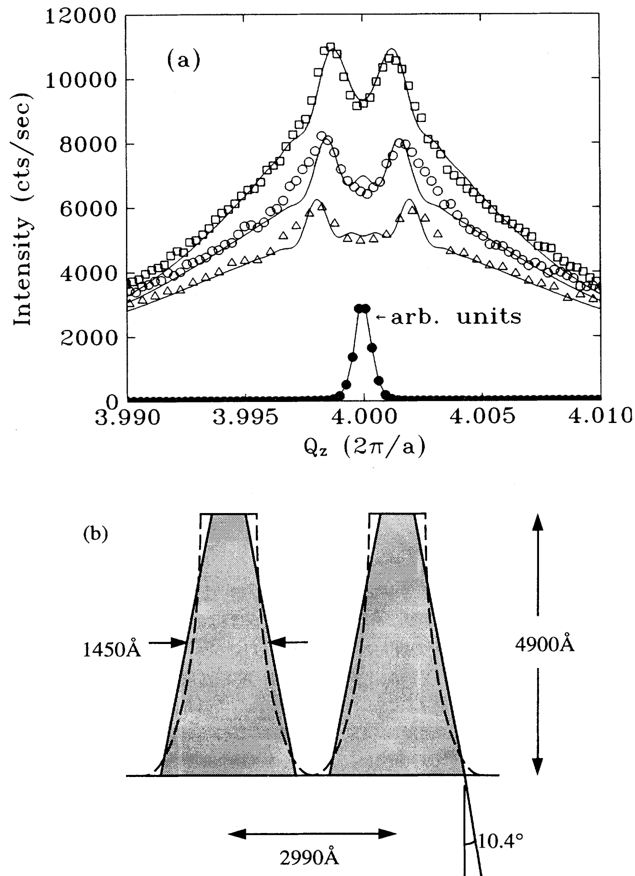

FIG. 5. (a) X-ray-diffraction intensity as a function of Q_z at $(4\tau/\sqrt{2}, -4\tau/\sqrt{2}, 4)$ (squares), $(5\tau/\sqrt{2}, -5\tau/\sqrt{2}, 4)$ (open circles), and $(6\tau/\sqrt{2}, -6\tau/\sqrt{2}, 4)$ (triangles) grating reflections around the (004). The solid curves are the calculated intensities using Eq. (3) and the grating shape shown in (b). For comparison, the (004) peak (filled circles) is also shown, in an arbitrary scale. (b) A trapezoid model (shaded region) for the grating shape. All the parameters are directly determined from our x-ray-diffraction experiment. To a good approximation, the trapezoid model resembles the real shape (dashed outline) as seen in the SEM picture (Fig. 2).

For epitaxial or heteroepitaxial growths on semiconductor grating surfaces, it is important to know how the grating lines are oriented and registered with respect to the crystallographic axes of the substrate. Here we demonstrate that such information is easily obtainable with x-ray diffraction. In our experiment, we first orient our sample in such a way that the ϕ axis of the four-circle diffractometer is parallel to the (004) direction of the crystal. Then we compare the ϕ angle at which a grating peak near the (004) shows a maximum intensity and the ϕ angle of an asymmetric Bragg reflection, e.g., $(1\bar{1}3)$. As shown in Fig. 6, the two ϕ scans at the $(5\tau/\sqrt{2}, -5\tau/\sqrt{2}, 4)$ and at the $(1\bar{1}3)$ exhibit a difference of 0.27° in their peak positions. We therefore conclude that the grating lines are almost parallel to the $[1\bar{1}0]$ axis with a slight misalignment of 0.27°.

The diffraction from a grating surface is closely related to the scattering from surface roughness, where a wide range of spatial frequencies may exist.[14] With a single spatial period in the experiment described here, the x-ray scattering is highly sensitive to possible imperfections in both the crystal lattice and the grating grid. For example, a variation in the grating period would introduce a broader grating interference peak. A loss of lateral atomic registry from one grating pillar to another would cause broader and diminishing grating peaks at larger momen-

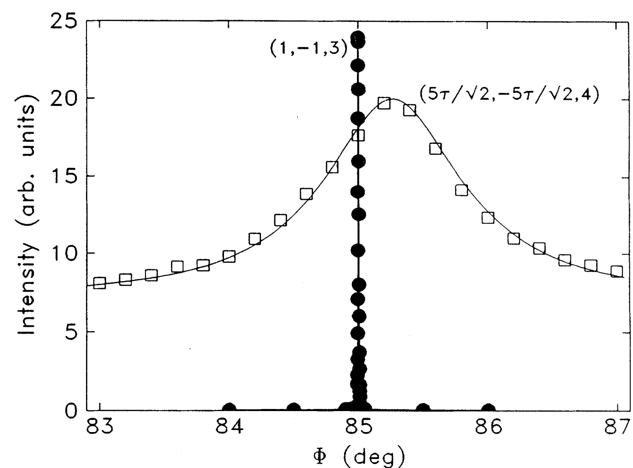

FIG. 6. Two ϕ scans to illustrate the grating orientation with respect to the crystal lattice. The filled circles are at the asymmetric Bragg reflection $(1,-1,3)$, and the open squares are at the grating reflection $(5\tau/\sqrt{2}, -5\tau/\sqrt{2}, 4)$. The solid curves are guides to the eye. The broad peak for the grating reflection is due to the wide out-of-plane resolution width ΔQ_χ.

tum transfers, i.e., at larger $|\mathbf{Q}|$'s. An atomic lattice relaxation in the grating layer would show a characteristically broadened or split Bragg peak. Information on atomic registry is important in the epitaxial growth of semiconductor overlayers, while lattice strain is of particular interest for heteroepitaxial structures such as $Al_xGa_{1-x}As$ and Si-Ge systems. Based on our experimental data, particularly the widths of the grating and Bragg peaks, we conclude that the lattice strain in our grating sample was below our detection level, $\Delta a/a \leq 3\times10^{-5}$, indicating high quality processing through the wet-acid-etching, electron-beam lithographic technique.

In summary, we have demonstrated that high-resolution x-ray diffraction on a mesoscopic single-crystal grating sample provides useful structural information with atomic scale precision. The sharp grating interference peaks due to the coherent illumination of the synchrotron radiation are highly sensitive to the grating parameters, such as period, width, and shape, as well as to atomic registry with the substrate and to crystal lattice strains. The technique can be applied not only to geometrically corrugated structures, but also to grating structures arising from periodic strains, composition modulations, or any other charge-density modulations on semiconductor surfaces. These features should be useful in probing fabricated structures[15] over a range of characteristic dimensions, epitaxial overlayers,[16] and perhaps self-assembled molecular structures.[17] With its broad applicable range we believe that x-ray diffraction will play a more important role in future studies of nanostructures and mesoscopic systems.

The authors would like to thank R. Bojko of the National Nanofabrication Facility at Cornell University for his assistance in fabricating our sample. This work was supported by the National Science Foundation through CHESS, under Grant No. DMR 90-21700, and through the Materials Science Center at Cornell University, under Grant No. DMR 91-21654.

[1] I. K. Robinson, in *Handbook on Synchrotron Radiation,* edited by D. E. Moncton and G. Brown (Elsevier, Amsterdam, 1991).

[2] W. P. Kirk and M. A. Reed, *Nanostructures and Mesoscopic Systems* (Academic, New York, 1992).

[3] M. E. Keeffe, C. C. Umbach, and J. M. Blakely, in *Interface Dynamics and Growth,* edited by K. S. Liang, M. P. Anderson, R. F. Bruinsmo, and G. Scoles, MRS Symposium Proceedings No. 237 (Materials Research Society, Pittsburgh, 1992).

[4] C. C. Umbach, M. E. Keeffe, and J. M. Blakely, J. Vac. Sci. Technol. A **9**, 1014 (1991).

[5] E. Colas, G. C. Nihous, and D. M. Hwang, J. Vac. Sci. Technol. A **10**, 691 (1992).

[6] B. E. Warren, *X-Ray Diffraction* (Addison-Wesley, New York, 1969).

[7] M. Born and E. Wolf, *Principles of Optics,* 6th ed. (Pergamon, New York, 1989).

[8] R. W. James, *The Optical Principles of the Diffraction of X-rays,* (Bell, London, 1948).

[9] S. R. Andrews and R. A. Cowley, J. Phys. C **18**, 6427 (1985).

[10] I. K. Robinson, Phys. Rev. B **33**, 3830 (1986).

[11] L. Tapfer and P. Grambow, Appl. Phys. A **50**, 3 (1990).

[12] A. T. Macrander and S. E. Slusky, Appl. Phys. Lett. **56**, 443 (1990).

[13] M. Sutton, S. G. J. Mochrie, T. Greytak, S. E. Nagler, L. E. Berman, G. A. Held, and G. B. Stephenson, Nature **352**, 608 (1991).

[14] S. K. Sinha, E. B. Sirota, S. Garoff, and H. B. Stanley, Phys. Rev. B **38**, 2297 (1988).

[15] K. D. Wise and K. Najafi, Science **254**, 1335 (1991).

[16] M. Sundaram, S. A. Chalmers, P. F. Hopkins, and A. C. Gossard, Science **254**, 1326 (1991).

[17] G. M. Whitesides, J. P. Mathias, and C. T. Seto, Science **254**, 1312 (1991).

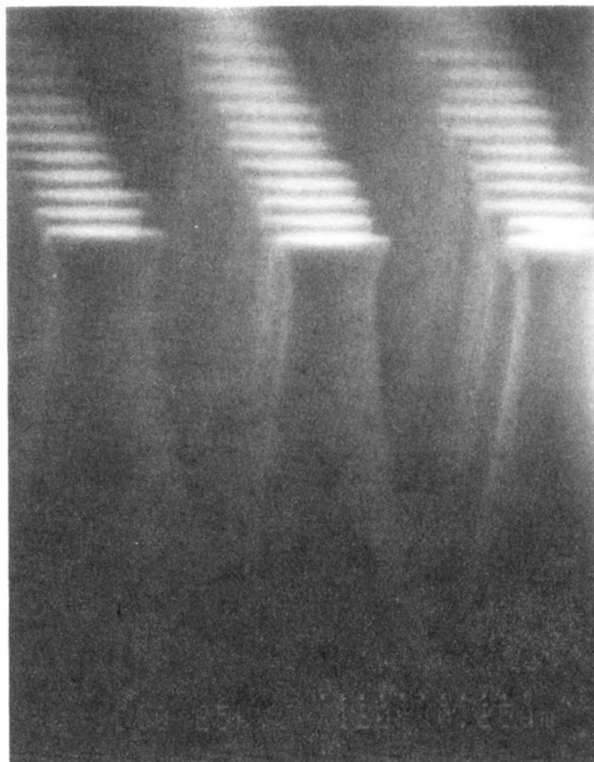

FIG. 2. A scanning electron micrograph (SEM) of a typical Si(001) grating surface studied in our x-ray-diffraction experiment. The nominal period of the grating is 0.3 μm.

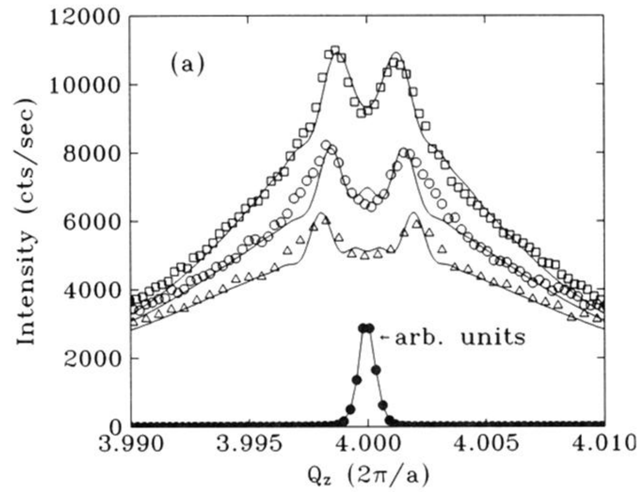

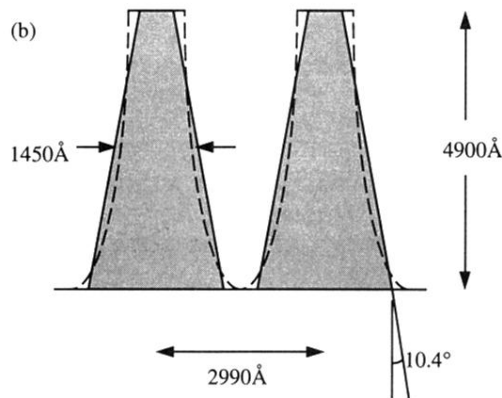

FIG. 5. (a) X-ray-diffraction intensity as a function of Q_z at $(4\tau/\sqrt{2}, -4\tau/\sqrt{2}, 4)$ (squares), $(5\tau/\sqrt{2}, -5\tau/\sqrt{2}, 4)$ (open circles), and $(6\tau/\sqrt{2}, -6\tau/\sqrt{2}, 4)$ (triangles) grating reflections around the (004). The solid curves are the calculated intensities using Eq. (3) and the grating shape shown in (b). For comparison, the (004) peak (filled circles) is also shown, in an arbitrary scale. (b) A trapezoid model (shaded region) for the grating shape. All the parameters are directly determined from our x-ray-diffraction experiment. To a good approximation, the trapezoid model resembles the real shape (dashed outline) as seen in the SEM picture (Fig. 2).